Journal of Metals, Materials and Minerals, 37(1), e2702, 2027

Effects of thermal oxidation and deposition time on the SERS activity of TiO_2 nanostructure films

Jutaporn WANNAPHUM[1], Watcharaporn THONGJOON[1], Chantana AIEMPANAKIT[2], Raumporn THONGRUANG[1], Montri AIEMPANAKIT[3], and Kamon AIEMPANAKIT[1,*]

[1] *Department of Physics, Faculty of Science and Technology, Thammasat University, Pathum Thani, 12121, Thailand*
[2] *Division of Physics, Faculty of Science and Technology Rajamangala University of Technology Thanyaburi, Pathum Thani, 12110, Thailand*
[3] *Department of Physics, Faculty of Science, Silpakorn University, Nakhon Pathom, 73000, Thailand*

***Corresponding author e-mail**: akamon@tu.ac.th

Received date:
31 March 2026
Revised date:
30 April 2026
Accepted date:
6 July 2026

Keywords:
TiO_2 films;
DC magnetron sputtering;
Thermal oxidation;
SERS;
OAD

Abstract

Titanium (Ti) nanostructure films were fabricated on glass substrates by DC magnetron sputtering using the oblique angle deposition (OAD) technique with varying deposition times. The as-deposited Ti films were subsequently oxidized in air at 400°C and 500°C to obtain TiO_2 nanostructure films. The effects of deposition time and oxidation temperature on the structural, morphological, and optical properties were systematically investigated and correlated with surface-enhanced Raman scattering (SERS) performance toward methylene blue (MB) molecules. Increasing both deposition time and oxidation temperature led to thicker films, larger grains, and enhanced crystallinity with higher surface roughness. The optical band gap gradually decreased as deposition time increased, a trend associated with microstructural evolution and improved crystallinity during thermal oxidation. Among all samples, the TiO_2 film oxidized at 400°C with a deposition time of 4 min exhibited the highest Raman enhancement, with a maximum enhancement factor (EF) of approximately 4.00 ± 0.064 (mean ± SD, n = 5), indicating that moderate oxidation promotes optimal nanostructured surface and charge-transfer efficiency. These findings highlight the important role of deposition time and oxidation conditions in governing the SERS activity of TiO_2 nanostructure films.

1. Introduction

Surface-Enhanced Raman Scattering (SERS) has attracted significant interest as an effective analytical technique for detecting molecules at ultra-low concentrations. Conventional SERS substrates typically rely on plasmonic mechanisms associated with noble metals such as gold (Au) and silver (Ag). However, their practical applications remain limited by insufficient chemical stability, poor reproducibility, and high fabrication costs.

To address these limitations, non-plasmonic SERS, based on charge-transfer interactions between semiconductor surfaces and target molecules, has emerged as a promising alternative. This approach offers enhanced signal stability and reproducibility. Consequently, various semiconductor materials have been extensively explored as non-plasmonic SERS substrates, including titanium dioxide TiO_2 [1–3], ZnO [4–7], SiO_2 [8–10], and graphene oxide [11–12].

Among these candidates, (TiO_2) has been widely investigated due to its high chemical stability, low toxicity, and structural versatility. TiO_2 can be fabricated into diverse nanostructures, such as nanorods [13–14], nanotubes [15–16], and nanoflowers [17], which provide increased specific surface area and tunable electronic band structures favorable for charge-transfer processes in non-plasmonic SERS systems. In particular, TiO_2 nanostructures, especially rutile nanostructures, have attracted considerable interest because their morphology and crystalline phase can be effectively tailored through seed-layer engineering and controlled growth conditions, enabling further optimization of their optical properties and SERS performance [18].

However, previous studies have shown that the SERS performance of TiO_2 is highly dependent on its crystal structure and surface properties. These characteristics can be effectively controlled through fabrication techniques [19–20] and post-deposition oxidation or annealing temperatures [21–22], which influence the crystalline phase, defect density, and surface electronic states, thereby affecting charge-transfer efficiency.

In this work, the effects of deposition time and oxidation temperature on the structural, morphological, optical, and SERS properties of TiO_2 nanostructure films fabricated by DC magnetron sputtering are systematically investigated and correlated with their SERS activity. This study focuses on elucidating the role of charge-transfer mechanisms in non-plasmonic SERS and provides insights into the development of stable and reliable semiconductor-based SERS substrates.

2. Experimental

Glass substrates (3 cm × 1 cm) were sequentially cleaned in acetone, methanol, and deionized water for 15 min each to remove organic and

particulate contaminants. An overview of the experimental procedure for the fabrication and characterization of TiO_2 films is schematically presented in Figure 1. After cleaning, titanium (Ti) films were deposited onto the glass substrates by DC magnetron sputtering using a high-purity titanium target (Ti, 99.995% purity; 2 inch diameter and 0.25 inch thickness; Kurt J. Lesker). The target–substrate distance was fixed at approximately 80 mm. Prior to deposition, the sputtering chamber was evacuated to a base pressure of ~5×10^{-5} mbar using diffusion and rotary pumps. During sputtering, high-purity argon gas (99.999%) was introduced at a flow rate of 15 sccm via a mass flow controller, resulting in a working pressure of ~1.9×10^{-3} mbar. The Ti target was pre-sputtered for 3 min in argon to remove surface oxides, and the sputtering power was maintained at 150 W.

To deliberately tailor the film morphology, an oblique-angle deposition (OAD) configuration was employed by tilting the substrates at 85° relative to the horizontal plane, as illustrated in Figure 2. This highly oblique geometry enhances atomic shadowing effects during film growth, thereby promoting anisotropic deposition and facilitating the formation of columnar nanostructures. Deposition times were systematically varied at 2 min, 4 min, 6 min, 8 min, and 10 min to investigate the effects of deposition time on the resulting film morphology and SERS activity.

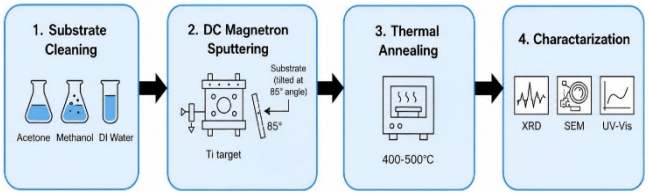

Figure 1. Schematic illustration of the experimental procedure.

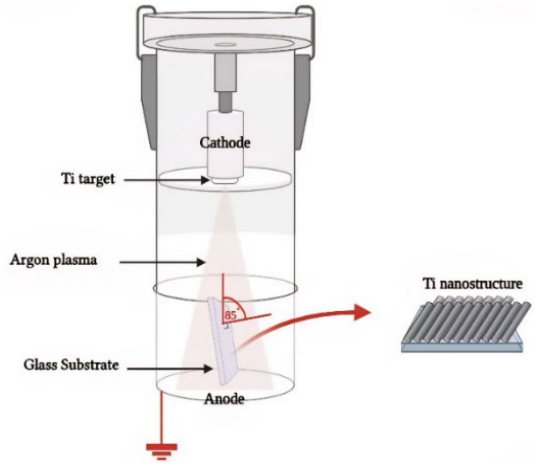

Figure 2. Schematic of oblique-angle deposition (85°) for TiO_2 thin-film growth.

Table 1. Deposition conditions for TiO_2 films.

Deposition time	Conditions of annealing temperature	
[min]	400°C	500°C
2	4Ti-2	5Ti-2
4	4Ti-4	5Ti-4
6	4Ti-6	5Ti-6
8	4Ti-8	5Ti-8
10	4Ti-10	5Ti-10

Subsequently, the as-deposited Ti films were thermally annealed in air at 400°C and 500°C for 1 h using a heating rate of approximately 12°C·min^{-1} to induce oxidation and structural transformation into TiO_2, as summarized in the experimental flowchart shown in Figure 1. The deposition conditions and sample codes are summarized in Table 1. The crystalline structure of the resulting TiO_2 films was characterized by X-ray diffraction (XRD) using Cu Kα radiation (λ = 1.54184 Å; Bruker D2 PHASER). Surface morphology was examined by field-emission scanning electron microscopy (FE-SEM; TESCAN MIRA-3, Czech Republic). In addition, optical transmittance spectra before and after annealing were recorded using a UV–Vis spectrophotometer (G10S UV–Vis, Thermo Scientific) over the wavelength range of 200 nm to 1000 nm. In addition, photoluminescence (PL) spectra were recorded using a photoluminescence spectrometer (HORIBA Scientific; instrument info: FLMAX-0539D-1022-FMPLUS R928P) over the wavelength range of 340 nm to 800 nm under identical instrumental conditions for samples to enable direct comparison of the emission behavior. Finally, the SERS activity of the TiO_2 films was evaluated using a Raman spectrometer (XploRA™PLUS by HORIBA Scientific).

3. Results and discussion

The as-deposited Ti films prepared at all deposition times (2 min to 10 min) do not exhibit distinct diffraction peaks characteristic of crystalline phases, indicating that the films are quasi-amorphous or composed of extremely fine nanocrystallites whose grain sizes are below the detection limit of XRD. This observation is consistent with previous studies reporting featureless or significantly broadened diffraction patterns for TiO_2 films prior to thermal annealing, which are attributed to an incompletely crystallized structure [23–25]. From the XRD results, it can therefore be inferred that the as-deposited films lack long-range structural order and remain in a metastable state, where thermal energy supplied during annealing is required to drive crystallization, grain growth, and phase evolution toward a more ordered TiO_2 structure.

Following annealing at 400°C, distinct diffraction peaks emerge that can be indexed to the rutile phase of TiO_2. The dominant reflection appears at a 2θ angle of approximately 27° to 28°, corresponding to the (110) crystallographic plane, while additional reflections are observed around 36° to 37°, which can be assigned to the (101) or (211) planes in accordance with the JCPDS database for rutile TiO_2. The intensity of these rutile-related peaks increases progressively as the deposition time is extended from 2 min to 10 min, indicating a continuous enhancement of crystallinity. The appearance of rutile TiO_2 at 400°C indicates that phase transformation occurred at a relatively low temperature, which may be attributed to the dense nanostructured morphology produced under the present sputtering conditions [26]. This behavior is likely related to the nanostructured thin-film geometry produced by oblique-angle sputtering, which introduces a high surface area, nonequilibrium growth characteristics, and a defect-rich micro-structure that can lower the activation barrier for oxidation and crystallization during annealing. Although anatase is more commonly reported for photocatalytic and SERS applications, the present results demonstrate that rutile TiO_2 can also provide effective non-plasmonic Raman enhancement when combined with suitable nanostructured surface and defect-assisted

charge-transfer pathways [27–28]. Such an evolution, characterized by the growth of diffraction intensity and the transformation from a quasi-amorphous structure to a polycrystalline state upon thermal treatment in the temperature range of approximately 300°C to 400°C, has been widely documented for TiO_2 thin films and is in good agreement with the behavior observed in the present study [30–31].

At a higher annealing temperature of 500°C, the XRD patterns exhibit rutile-phase diffraction peaks that are noticeably sharper and more intense than those observed at 400°C. The narrowing of the rutile-related diffraction peaks at elevated annealing temperatures qualitatively reflects the suppression of structural disorder and the promotion of crystallite growth within the TiO_2 films. This behavior is consistent with previous reports describing thermally induced grain growth and improved crystallinity in TiO_2 thin films. Furthermore, extending the deposition time leads to a continuous increase in the intensity of such rutile reflections, which can be attributed to an enhanced crystalline fraction and increased film thickness [32–34].

Figure 4–5 present the top-view and cross-sectional FE-SEM images of the TiO_2 films prepared under different deposition times and annealing temperatures. The observed morphological variations provide experimental evidence for the role of surface structure in governing the SERS response of the films.

For the films annealed at 400°C, the sample deposited for 2 min (Figure 4(a)) shows a relatively smooth surface with very fine grains, where individual grain boundaries are not clearly resolved [35]. This morphology is consistent with the weak XRD features observed for short deposition times and suggests a structure that remains close to a quasi-amorphous state. Despite the limited crystallinity, the surface may contain structural disorder and defect-related sites, which can contribute to molecular adsorption and interfacial charge-transfer processes [36–37].

With increasing deposition time from 4 min to 10 min (Figure 4(b–e)), the surface grains become progressively more distinguishable and exhibit gradual coalescence. This evolution reflects increased film thickness and partial crystallite growth while maintaining a heterogeneous nanoscale surface. Among these samples, the film deposited for 4 min exhibits moderate grain development while retaining a relatively high density of grain boundaries and surface imperfections. This structural condition is favorable for SERS, as it supports efficient adsorption of probe molecules and facilitates defect-assisted charge transfer between TiO_2 and the adsorbates [38].

In contrast, the films annealed at 500°C exhibit more pronounced grain growth and surface densification (Figure 4(f–j)). At deposition times of 4 min and 6 min, larger and more compact nanograins are formed, indicating enhanced crystallization induced by the higher annealing temperature [39]. Further extension of the deposition time leads to a denser surface morphology with reduced nanoscale heterogeneity. Cross-sectional images (Figure 5) reveal increased film thickness and more pronounced columnar grain growth at 500°C, suggesting enhanced atomic diffusion and structural rearrangement during annealing.

Although higher annealing temperatures improve crystallinity, the accompanying reduction in grain-boundary population and possible decrease in defect-related surface states appear to be detrimental to SERS performance. Excessive grain coalescence reduces the number of active sites for molecular adsorption and suppresses charge-transfer interactions essential for non-plasmonic Raman enhancement [40–42]. Consequently, films annealed at 400°C, particularly those deposited for 4 min, exhibit superior SERS activity compared with their 500°C counterparts.

The UV–Vis optical transmittance spectra of the TiO_2 films annealed at 400°C and 500°C are presented in Figure 6(a–b), respectively. For the films annealed at 400°C, all samples exhibit similar spectral profiles, with a pronounced absorption edge located at approximately 350 nm to 400 nm, corresponding to the electronic transition from the valence band to the conduction band of rutile TiO_2. The primary variation among the samples lies in the transmittance levels within the visible to near-infrared (Vis–NIR) region, which generally increase with deposition time from 2 min to 8 min, followed by a slight decrease at 10 min. This trend reflects the combined influence of increasing film thickness and light scattering associated with the surface morphology evolution during deposition, which alters the optical path and effective absorption [43–44].

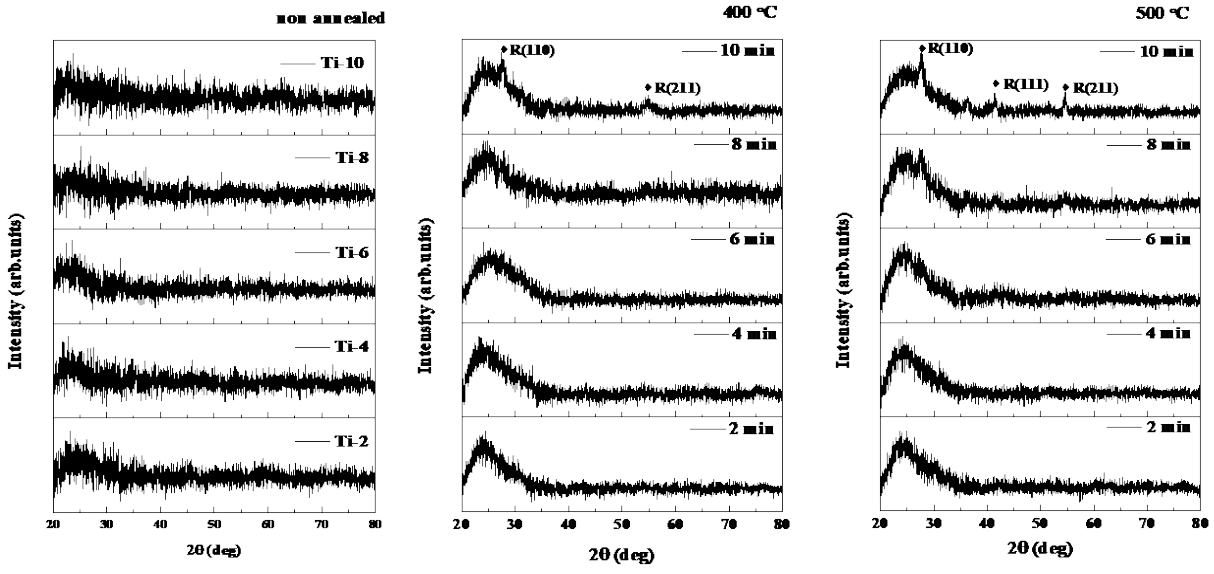

Figure 3. XRD patterns of TiO_2 films prepared by DC magnetron sputtering with deposition times of 2 min to 10 min before and after annealing at 400°C and 500°C.

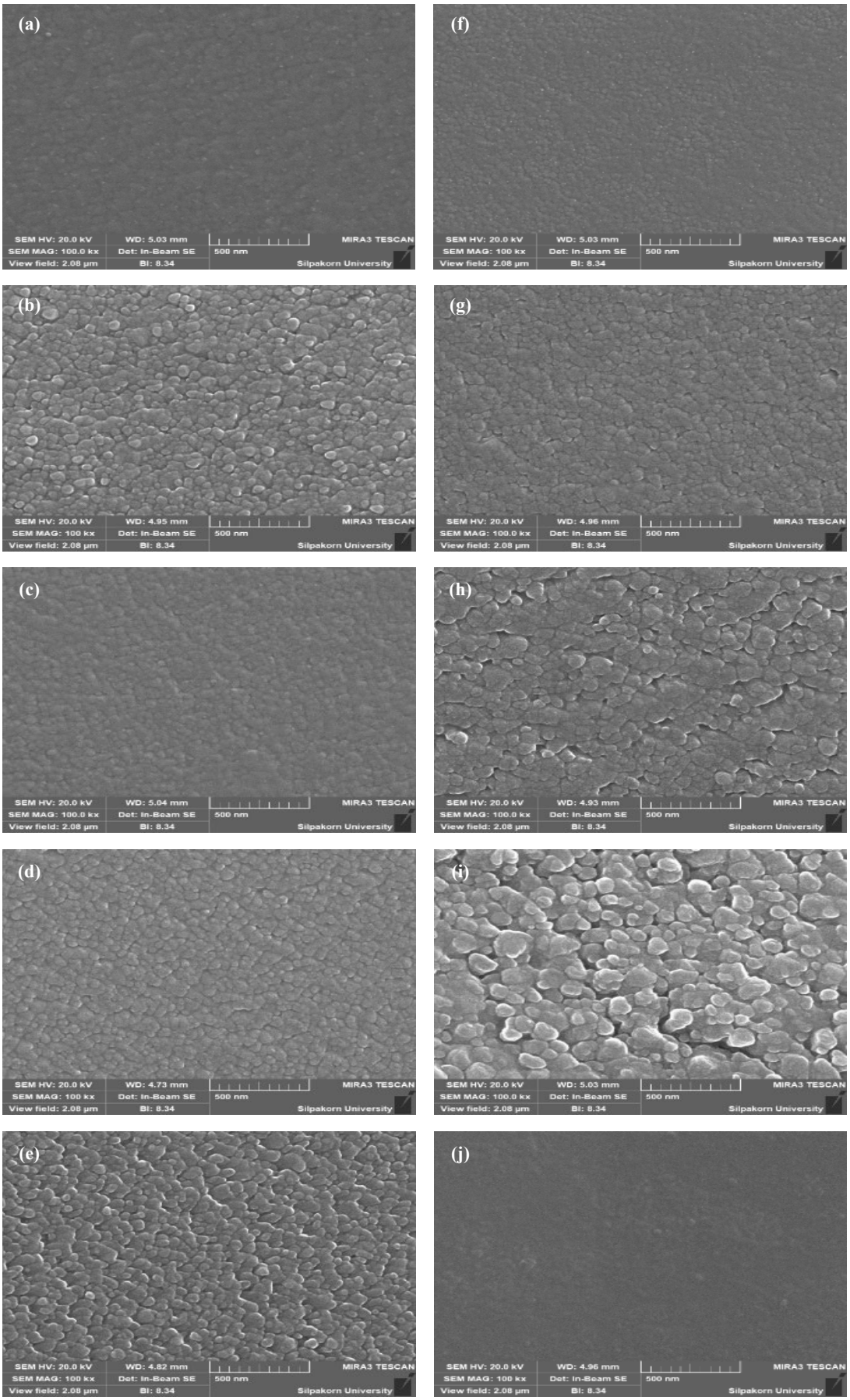

Figure 4. Top-view FE-SEM images of TiO_2 films deposited at different times and annealed at (a–e) 400°C and (f–j) 500°C. The deposition times are 2 min, 4 min, 6 min, 8 min, and 10 min for panels (a–e) and (f–j), respectively. The scale bar in all images is 500 nm.

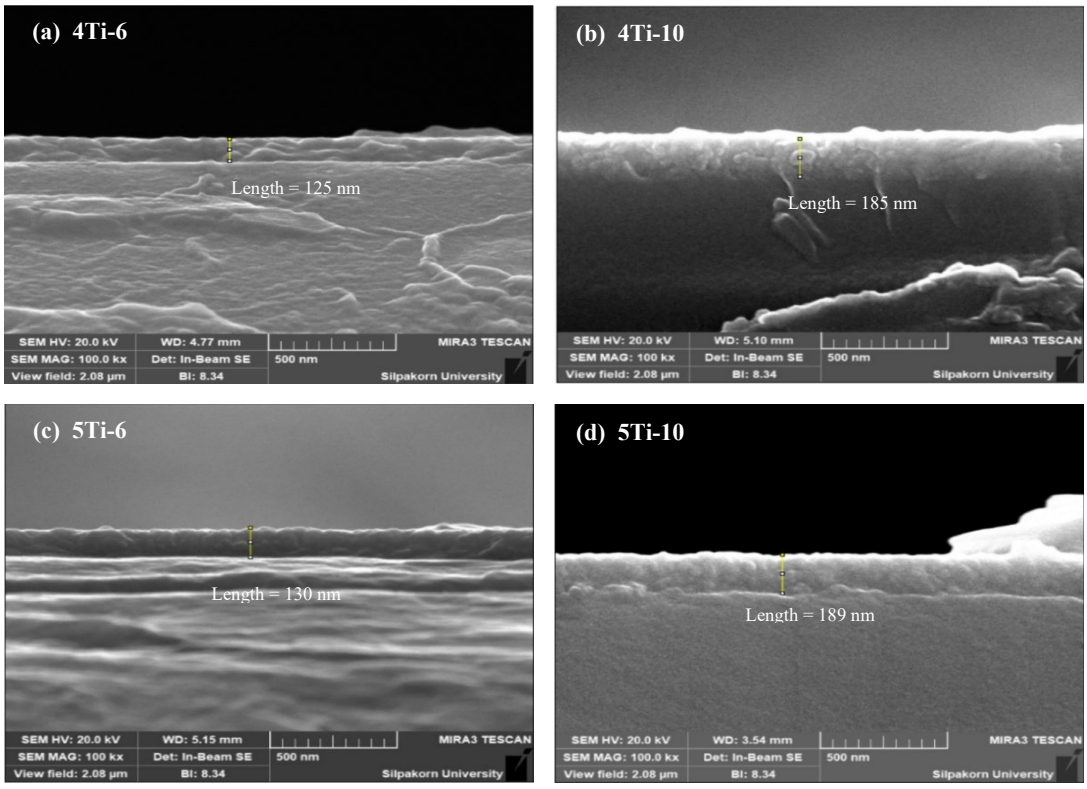

Figure 5. Cross-sectional FE-SEM images of TiO_2 films deposited for 6 min and 10 min and annealed at (a–b) 400°C and (c–d) 500°C. Panels (a) and (b) correspond to the 6 min and 10 min deposition samples annealed at 400°C, respectively, whereas panels (c) and (d) correspond to the 6 min and 10 min deposition samples annealed at 500°C, respectively. The scale bar in all images is 500 nm.

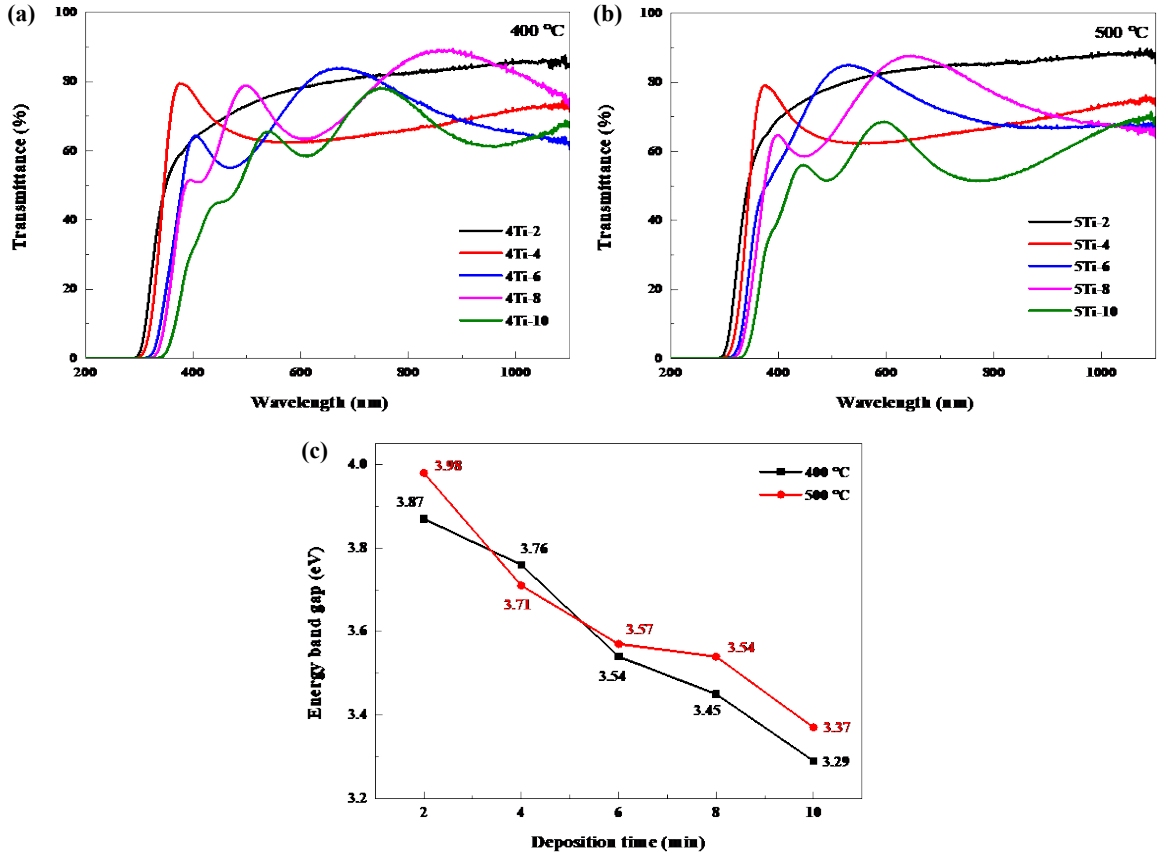

Figure 6. UV–Vis optical transmittance spectra in the wavelength range of 200 nm to 1100 nm for TiO_2 films deposited for 2 min to 10 min and annealed at (a) 400°C, and (b) 500°C. Panel (c) shows the indirect optical band gap values determined from the corresponding Tauc plots.

For the films annealed at 500°C, the overall transmittance spectra are qualitatively similar to those of the 400°C samples, but display slightly higher transmittance across the Vis region, which may be associated with enhanced crystallinity and a lower concentration of defect-related states after high-temperature annealing. An incremental redshift of the absorption edge is observed as deposition time increases, suggesting a modest reduction in the optical band gap (Figure 6(b)), likely associated with microstructural evolution and improved structural ordering at elevated temperatures [45–46].

The indirect optical band gap (E_g) values were determined from the corresponding Tauc plots using the relation:

$$(\alpha h\nu)^{1/2} = A\left(h\nu - E_g\right) \quad (1)$$

where α is the absorption coefficient, $h\nu$ is the photon energy, and A is a proportionality constant. As shown in Figure 6(c), the films annealed at 400°C exhibit a gradual decrease in E_g from ~3.87 eV for the 2 min deposition to ~3.29 eV for the 10 min deposition. In comparison, the films annealed at 500°C show slightly higher band gap values across all deposition conditions, ranging from ~3.98 eV (2 min) to ~3.37 eV (10 min). The calculated optical band gap values of the TiO_2 nanostructure films range from approximately 3.29 eV to 3.98 eV, which are slightly higher than the typical values reported for bulk rutile (~3.0 eV) and anatase (~3.2 eV) TiO_2. This blue shift may be associated with the combined effects of microstructural disorder, defect-related states, and size-dependent electronic effects commonly observed in nanostructured TiO_2 thin films. In particular, the OAD promotes nonequilibrium growth, leading to a defect-rich nanostructure that may modify the electronic structure and shift the absorption edge toward higher energies. Such microstructure-dependent variations in the optical band gap have been widely reported for TiO_2 thin films [47], as changes in grain size and microstructure significantly influence the band gap energy [48–49]. Furthermore, as the band gap values were extracted using the indirect-transition Tauc model, the obtained results should be interpreted as the optical band gap of the present nanostructured thin films rather than the intrinsic band gap of ideal bulk TiO_2.

The relatively large optical band gap values observed in this study are likely influenced by thin-film geometry, nanostructured morphology, and defect-related states inferred from the structural and optical analyses. However, further detailed spectroscopic investigations would be required to quantitatively identify the dominant contribution.

The Raman spectra of methylene blue (MB) at a concentration of 0.01 mM (10 µL) on TiO_2 nanostructure films are presented in Figure 7. For the films annealed at 400°C (4Ti series, Figure 7(a)), all samples display the characteristic vibrational features of MB, with a prominent band observed at approximately 1620 cm^{-1}, corresponding to aromatic ring vibrations and C–C/C–N stretching modes within the MB molecule [50–51]. The intensity of this peak increases significantly as the deposition time extends from 2 min to 4 min, indicating that the surface morphology obtained at a deposition time of 4 min is more favorable for molecular adsorption and interfacial charge-transfer processes. When the deposition time exceeds 4 minutes (6 min to 10 min), the Raman peak intensity slightly decreases, suggesting that excessive grain coalescence and densification reduce the availability of surface sites and localized charge-transfer enhancement, thereby diminishing the SERS enhancement [52–53].

In contrast, the films annealed at 500°C (5Ti series, Figure 7(b)) exhibit lower overall Raman intensities, although the main MB band at ~1620 cm^{-1} remains clearly detectable under all deposition conditions. This reduction in SERS performance can be correlated with the increased grain size, enhanced crystallinity, and slightly larger band gap values (Figure 6(c)), which may reduce the availability of defect-related surface states and nanoscale surface heterogeneity. These factors limit both the number of active adsorption sites and the formation of localized charge-transfer enhancement, thereby suppressing charge-transfer interactions between TiO_2 and MB.

Overall, a comparison of the two annealing temperatures indicates that the highest SERS activity is achieved for the films annealed at 400°C with an intermediate deposition time of 4 min. This optimal condition provides a combination of moderate film thickness and nanostructured morphology that appears favorable for molecular adsorption and interfacial charge-transfer processes. These observations are consistent with the morphological and optical analyses discussed previously, highlighting the crucial interplay between nanoscale structure, defect states, and optical properties in governing SERS performance [54–55].

The quantitative evaluation of the SERS activity of the TiO_2 nanostructure films is summarized in Figure 8, which presents the enhancement factor (EF) as a function of deposition time and annealing temperature. In this work, the EF was calculated using the following expression:

$$EF = \frac{I_{SERS}}{C_{SERS}} \times \frac{C_{RS}}{I_{RS}} \quad (2)$$

The *EF* of the TiO_2 nanostructure films was calculated using Equation (2), where ISERS and IRS are the Raman intensities of methylene blue (MB) measured on the TiO_2 substrate and in the reference solution, respectively, and CSERS and CRS are the corresponding MB concentrations. In this work, the *EF* was determined from the characteristic Raman band at 1620 cm^{-1}, which is assigned to aromatic ring vibrations and C–C stretching modes of MB. The SERS measurements were performed using a 532 nm laser, a 50× objective lens, and an acquisition time of 5 s. This formulation accounts for differences in analyte concentration and provides a normalized measure of the Raman signal enhancement arising from the nanostructured surface of films. The reference Raman signal was collected under the same instrumental conditions for the corresponding MB reference solution, and the MB concentration was 0.01 mM [56–58].

As shown in Figure 8, the TiO_2 films annealed at 400°C exhibit higher *EF* values across all deposition times compared with films annealed at 500°C. Among the 400°C series, the film deposited for 4 min (4Ti-4) reaches the maximum *EF* of approximately 4.01 ± 0.064 (mean ± SD, n = 5), consistent with the most intense Raman peak of methylene blue (MB) observed at ~1620 cm^{-1} in Figure 7(a). When the deposition time is further extended to 6 min, 8 min, and 10 min, the *EF* gradually decreases to 3.27, 2.95, and 1.16, respectively. This trend aligns with the corresponding Raman spectra, where both the intensity of the main MB peak and the spectral background diminish. The reduction in EF at longer deposition times may be associated with increased grain coalescence and film densification, which are less favorable for molecular adsorption and interfacial charge-transfer processes.

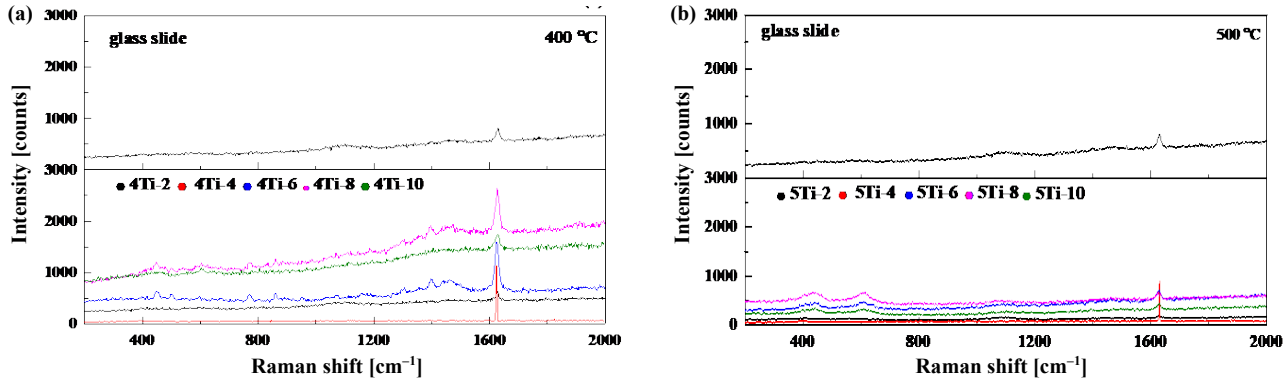

Figure 7. Raman spectra of methylene blue (MB) at a concentration of 0.01 mM (10 µL) measured on TiO_2 nanostructure films prepared with deposition times of 2 min, 4 min, 6 min, 8 min, and 10 min and subsequently oxidized at (a) 400°C, and (b) 500°C.

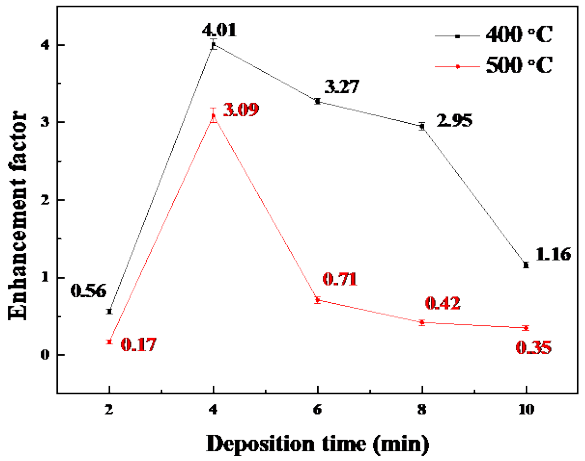

Figure 8. Enhancement factor (EF) of TiO_2 nanostructure films prepared with deposition times of 2 min, 4 min, 6 min, 8 min, and 10 min and subsequently oxidized at 400°C and 500°C. Data are presented as mean ± SD from five replicate measurements at randomly selected positions.

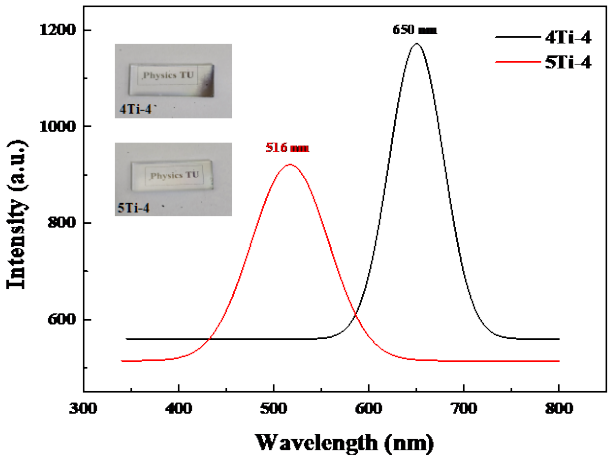

Figure 9. Photoluminescence (PL) spectra of TiO_2 films annealed at 400°C (4Ti-4) and 500°C (5Ti-4).

For the films annealed at 500°C, the maximum EF (~3.09) is also observed at a deposition time of 4 min; however, this value is markedly lower than that of the 400°C counterpart. As the deposition time increases to 6 min, 8 min, and 10 min, the *EF* drops sharply to 0.71, 0.42, and 0.35, consistent with the weak Raman intensities and flattened spectral backgrounds shown in Figure 7(b). Although the enhancement factors are lower than those typically reported for plasmonic SERS substrates, the obtained values are reasonable for non-plasmonic TiO_2 systems, where Raman enhancement is primarily governed by interfacial charge-transfer mechanisms. The observed decline in SERS performance may be associated with the higher crystallinity and slightly increased optical band gap (Figure 6(c)) induced by the elevated annealing temperature, which could reduce the contribution of defect-related electronic states to charge-transfer interactions between TiO_2 and MB molecules. Furthermore, pronounced grain growth and coalescence at 500°C result in smoother film surfaces with fewer nanoscale junctions and defect sites, thereby limiting the formation of localized charge-transfer pathways at defect-rich surface interfaces and suppressing efficient Raman signal enhancement.

Overall, the combination of Raman spectral data, FE-SEM morphological analysis, and optical band gap measurements indicates that the most favorable conditions for SERS arise in films annealed at 400°C with an intermediate deposition time of 4 min. Under these conditions, the TiO_2 films exhibit a nanostructured morphology and moderate film thickness that appear favorable for molecular adsorption and interfacial charge-transfer processes, resulting in enhanced Raman signals. This mechanistic insight emphasizes the importance of controlling both structural and electronic features in engineering TiO_2-based SERS substrates.

It should be noted that the present discussion is based on qualitative morphological observations. Further quantitative characterization of defect-related states would be beneficial for confirming the proposed charge-transfer mechanism.

To further investigate the role of defect-related states in the TiO_2 films, PL spectroscopy was performed, as shown in Figure 9. The broad visible PL bands centered at approximately 516 nm and 650 nm are consistent with defect-related emissions in TiO_2. In particular, previous studies have shown that visible PL in TiO_2 is associated with surface and subsurface oxygen vacancies, shallow and deep trap states, and mid-gap electronic states that participate in radiative recombination pathways. The appearance of these bands suggests that the present TiO_2 films contain defect-related states that may influence the electronic processes occurring at the film surface. In the context of the present work, such states may contribute to the formation of intermediate energy levels that facilitate interfacial charge-transfer interactions between TiO_2 and MB molecules. This interpretation is consistent

with the Raman and *EF* results, where the films annealed at 400°C, particularly the 4 min deposition sample, exhibited the strongest SERS response. The enhanced performance of this sample may be associated with the combined effects of nanostructured morphology and defect-related electronic states, which are favorable for molecular adsorption and interfacial charge-transfer processes at the TiO_2/MB interface [59–60].

4. Conclusions

TiO_2 nanostructure films were successfully fabricated on glass substrates by DC magnetron sputtering using oblique-angle deposition and subsequently oxidized at 400°C and 500°C. The effects of deposition time and annealing temperature on the structural, morphological, optical, and photoluminescence properties of the films were systematically investigated and correlated with their SERS activity toward methylene blue (MB). XRD and FE-SEM analyses revealed that thermal oxidation promoted crystallization and nanocluster formation, with thicker films and larger grains observed at longer deposition times and higher annealing temperatures. UV–Vis and Tauc plot analyses showed that the optical band gap decreased with increasing deposition time, which was associated with microstructural evolution during thermal oxidation. In addition, PL spectroscopy exhibited broad visible emission bands centered at approximately 516 nm and 650 nm, suggesting the presence of defect-related states that may participate in radiative recombination and influence interfacial electronic processes at the TiO_2 surface. SERS measurements demonstrated that the films annealed at 400°C consistently exhibited stronger Raman enhancement than those annealed at 500°C, with the 4 min deposition sample (4Ti-4) showing the highest enhancement factor of approximately 4.01. This superior performance may be associated with a favorable combination of moderate film thickness, nanostructured morphology, and defect-related electronic interactions at the TiO_2/MB interface. Overall, the results demonstrate that careful control of deposition time and annealing temperature is essential for tuning the structural and electronic properties of TiO_2 nanostructure films and optimizing their non-plasmonic SERS activity.

Acknowledgments

This study was supported by Thammasat University Research Fund, Contact No. TUFT 049/2569. The author gratefully acknowledges the Full Scholarship for Research, Internationalization, and Education, Thammasat University, for the Academic Year 2567.

References

[1] L. Yang, X. Jiang, W. Ruan, B. Zhao, W. Xu, and J. R. Lombardi, "Charge-transfer induced surface-enhanced Raman scattering on Ag–TiO_2 nanoparticles," *Journal of Physical Chemistry C*, vol. 113, no. 39, pp. 16226–16231, 2009.

[2] T. Rajh, N. M. Dimitrijevic, M. Bissonnette, T. Koritarov, and V. Konda, "SERS of nanoparticles (TiO_2 hybrid composites)," *Journal of the American Chemical Society*, vol. 131, no. 32, pp. 12090–12091, 2009.

[3] Z. Zhao, and H. Xu, "Charge-transfer process in surface-enhanced Raman scattering on semiconductor nanomaterials," *Nanomaterials*, vol. 11, no. 8, p. 2110, 2021.

[4] S. Yang, J. Yao, Y. Quan, M. Hu, R. Su, M. Gao, D. Han, and J. Yang, "Monitoring the charge-transfer process in a Nd-doped ZnO semiconductor SERS substrate," *Light: Science and Applications*, vol. 9, p. 128, 2020.

[5] T. T. Tran, B. D. Nguyen, T. T. Pham, T. C. Doan, H. V. Pham, T. T. Nguyen, and D. D. Nguyen, "Study of charge transfer contribution to surface-enhanced Raman scattering on octahedral Cu_2O nanostructures," *Vietnam Journal of Chemistry*, vol. 60, no. 4, pp. 491–499, 2022.

[6] N. T. Phuc, N. V. Duy, and N. V. Hieu, "Increasing charge transfer of SERS by the combination of two semiconductors in Ag/a-Al_2O_3-Al/ZnO nanostructures," *RSC Advances*, vol. 13, no. 18, pp. 10237–10247, 2023.

[7] J. F. Arenas, I. López-Tocón, J. C. Otero, and J. I. Marcos, "Charge-transfer processes in surface-enhanced Raman scattering: Franck–Condon active vibrations of pyrazine," *Journal of Physical Chemistry*, vol. 100, no. 41, pp. 16410–16416, 1996.

[8] M. A. Apostolaki, M. Farsari, M. Vamvakaki, and A. Ranella, "Interplay of plasmonic and charge transfer effects for SERS in WO_3/TiO_2 inverse opal films with Ag nanoparticles," *Materials Advances*, vol. 6, pp. 27–38, 2025.

[9] Y. Fang, X. Li, H. Wang, and J. Zhang, "Uniform 3D SERS substrate SiO_2, AuAg collaborate with target-mediated DNA network structure as a signal amplifier for ultrasensitive detection of miRNA-21," *Sensors and Actuators, B: Chemical*, vol. 288, p. 117777, 2025.

[10] J. Li, Q. Chen, Y. Xu, X. Zhang, and Y. Wang, "Fabrication and SERS performance of SiO_2, Ag core–shell nanoparticle arrays," *Journal Nanophotonics*, vol. 20, pp. 8131–8144, 2025.

[11] M. V. Zamarripa, A. A. Rivera, U. Sierra, P. Salas, A. H. Serafín-Muñoz, and G. Ramírez-García, "Improved charge-transfer resonance in graphene oxide/ZrO_2 substrates for plasmonic-free SERS determination of methyl parathion," *Chemosphere*, vol. 320, p. 137974, 2023.

[12] K. Pupel, Ł. Bujak, A. Święch, and A. Kamińska, "Direct SERS detection of folic acid using modified graphene oxide–gold nano-bowl composites," *ACS Omega,* vol. 9, no. 48, pp. 59351–59364, 2024.

[13] S. Li, S. Yang, Y. Chen, L. Sun, H. Zhang, and H. Xu, "TiO_2 compact layer induced charge transfer enhancement in three-dimensional TiO_2-Ag SERS substrates," *Journal of Materials Chemistry C*, vol. 11, pp. 8270–8280, 2023.

[14] N. Serginay, E. Yilmaz, A. Yildirim, and M. Ozdemir, "Silver nanostructure-decorated hierarchical titanium dioxide nanostructures for highly sensitive SERS detection," *Applied Surface Science*, vol. 610, p. 155466, 2023.

[15] H. Zhai, C. Zhu, X. Wang, Y. Yuan and H. Tang, "Arrays of Ag-nanoparticles decorated TiO_2 nanotubes as reusable three-dimensional surface-enhanced Raman scattering substrates for molecule detection," *Frontiers in Chemistry*, vol. 10, p. 992236, 2022.

[16] M. Pisarek, M. Krawczyk, M. Hołdynski,´ R. Ambroziak, K. Bienkowski,´ A. Roguska, J. Krajczewski, and A. Kudelski, " Hybrid nanostructures based on TiO_2 nanotubes with Ag, Au, or bimetallic Au−Ag deposits for Surface-Enhanced Raman Scattering (SERS) Applications," *Journal of Physical Chemistry C*, vol. 127, pp. 24200−24210, 2023.

[17] W. Yang, Q. Ou, C. Li, M. Cheng, W. Li, and Y. Liu, "Ultra-sensitive flower-like TiO_2/Ag substrate for SERS detection of pigments and melamine," *RSC Advances*, vol. 12, pp. 6958–6965, 2022.

[18] J. Wu, S. Lo, K. Song, B. K. Vijayan, W. Li, K. A. Gray, and V. P. Dravid, "Growth of rutile TiO_2 nanostructures on anatase TiO_2 thin films on Si-based substrates," *Journal of Materials Research*, vol. 26, no. 13, pp. 1646–1652, 2011.

[19] Z. Ding, L. Zhang, W. Xu, J. Li, Y. Wang, and L. Chen, "Ag array SERS substrate for quantitative and multiplex analysis based on TiO_2 nanostructure-Ag hybrid structures," *RSC Advances*, vol. 13, pp. 8270–8280, 2023.

[20] S. A. A. Anaam, and M. Z. Sahdan, "Precursor-concentration-controlled morphology of TiO_2 nanorod/nanoflower films for enhanced photoelectrochemical water splitting and investigating their growth mechanism," *Bulletin of Chemical Reaction Engineering and Catalysis*, vol. 19, pp. 15–31, 2024.

[21] A. Tighineanu, T. Ruff, S. Albu, R. Hahn, and P. Schmuki, "Conductivity of TiO_2 nanotubes: Influence of annealing time and temperature," *Chemical Physics Letters*, vol. 494, pp. 260–263, 2010.

[22] L. Noel, A. Khitous, C. Molinaro, H. W. Zan, D. Berling, F. Grasset, and O. Soppera, "Laser direct writing of crystallized TiO_2 by photothermal effect induced by gold nanoparticles," *Advanced Materials Technologies*, vol. 9, p. 2300407, 2024.

[23] S. Kumar, H. Sharma, J. Yadav, J. Prasad, and M. Singh, "TiO_2 thin films fabrication and characterization in response to heat treatment," *Oriental Journal of Chemistry,* vol. 40, no. 4, pp. 1109–1115, 2024.

[24] N. R. Mathews, E. R. Morales, M. A. Cortés-Jacome, and J. A. Toledo Antonio, "TiO_2 thin films-influence of annealing temperature on structural, optical and photocatalytic properties," *Solar Energy*, vol. 83, no. 6, pp. 1499–1508, 2009.

[25] N. Chaabia, D. Abdi, A. Kamarchou, A. Berchi, F. Rahal, and S. Benhamida, "Preparation of amorphous and crystalline titanium dioxide on FTO: ITS characterization and photo-catalytic effect on eriochrome black T," *Journal of Nanomaterials and Biostructures*, vol. 16, no. 4, pp. 1235–1242, 2021.

[26] C. Aiempanakit, and K. Aiempanakit, "Structural development and phase transformation behavior of thermally-oxidization Ti by sputtering power and OAD technique," *Materials Chemistry and Physics*, vol. 280, p. 125814, 2022.

[27] W. Shi, J. C. Lin, R. Da, R. Li, Z. Li, Z. Feng, L. Lin, R. Zhang, and Z. Wang, "UV-irradiated and SPS-constructed vacancy-rich CO-doped TiO_2 for highly sensitive SERS detection via enhanced charge transfer," *ACS Applied Materials and Interfaces*, vol. 17, no. 39, pp. 55576–55586, 2025.

[28] S. K. Islam and A. Ponte, "Charge-transfer and SERS coupling on TiO_2," *American Journal of Analytical Chemistry*, vol. 14, no. 11, pp. 519–530, 2023.

[29] J. Saari, H. Ali-Löyty, K. Lahtonen, M. Hannula, L. Palomäki, A. Tukiainen, and M. Valden, "Low-temperature route to direct amorphous to rutile crystallization of TiO_2 thin films grown by atomic layer deposition," *The Journal of Physical Chemistry C*, vol. 126, no. 36, pp. 15357–15366, 2022.

[30] V. T. Lukong, K. Ukoba, K. O. Yoro, and T. C. Jen, "Annealing temperature variation and its influence on the self-cleaning properties of TiO_2 thin films," *Heliyon*, vol. 8, p. e09048, 2022.

[31] A. A. Al-Samarai, "Structural and optical properties of annealed TiO_2 powder prepared by sol-gel method," *Engineering And Technology Journal*, vol. 41, no. 12, pp. 1683–1693, 2023.

[32] A. R. Kamrosni, C. H. Dewi Suryani, A. Azliza, A. B. A. M. Mustafa, M. S. M. A. Anuar, M. Norsuria, V. Chobpattana, L. Kaczmarek, B. Jez, and M. Nabialek, "Microstructural studies of Ag/TiO_2 thin film; effect of annealing temperature on surface roughness and crystallite size," *Archives of Metallurgy and Materials*, vol. 67, no. 1, pp. 241–245, 2022.

[33] L. He, D. R. T. Zahn, and T. I. Madeira, "Photocatalytic performance of sol-gel prepared TiO_2 thin films annealed at different temperatures," *Materials*, vol. 16, p. 5494, 2023.

[34] S. D. Al-Algawi, R. T. Rasheed, and Z. R. Rhoomi, " Structural and optical properties of annealed TiO_2 powder synthesized by hydrothermal method," *Iraqi Journal of Science*, vol. 58, no. 3C, pp. 1683–1693, 2017.

[35] Y. Alaya, R. Souissi, M. Toumi, M. Madani, L. El Mir, N. Bouguila, and S. Alaya, "Annealing effect on the physical properties of TiO_2 thin films deposited by spray pyrolysis," *RSC Advances*, vol. 13, no. 32, pp. 21852–21860, 2023.

[36] Z. Zhao, M. Zhang, and X. Sun, "Charge-transfer process in surface-enhanced Raman scattering based on energy level locations of rare-earth Nd^{3+}-doped TiO_2 nanoparticles," *Nano-materials*, vol. 11, no. 8, p. 2063, 2021.

[37] L. Yang, X. Jiang, W. Ruan, B. Zhao, W. Xu, and J. R. Lombardi, "Observation of enhanced Raman scattering for molecules adsorbed on TiO_2 nanoparticles: Charge-transfer contribution," *Journal of Physical Chemistry C*, vol. 112, no. 50, pp. 20095–20098, 2008.

[38] Q. Chen, M. Betker, C. Harder, C. J. Brett, M. Schwartzkopf, N. M. Ulrich, M. E. Toimil-Molares, C. Trautmann, L. D. Söderberg, C. L. Weindl, V. Körstgens, P. Müller-Buschbaum, M. Ma, and S. V. Roth, "Biopolymer-templated deposition of ordered and polymorph titanium dioxide thin films for improved surface-enhanced raman scattering sensitivity," *Advanced Functional Materials*, vol. 32, no. 8, p. 2108556, 2022.

[39] W. Kaewwiset, W. Onreabroy, and P. Limsuwan, "Effect of annealed temperatures on the morphology of TiO_2 films," *Kasetsart Journal (Natural Science)*, vol. 42, pp. 341–345, 2008.

[40] S. Prucnal, R. Gago, D. G. Calatayud, L. Rebohle, M. O. Liedke, M. Butterling, A. Wagner, M. Helm, and S. Zhou, "TiO_2 phase engineering by millisecond range annealing for highly efficient photocatalysis," *Journal of Physical Chemistry C*, vol. 127, no. 26, pp. 12686–12694, 2023.

[41] M. Rogala, G. Bihlmayer, P. Dabrowski, C. Rodenbücher, D. Wrana, F. Krok, Z. Klusek, and K. Szot , "Self-reduction of the

native TiO_2 (110) surface during cooling after thermal annealing – in- operando investigations," *Scientific Reports*, vol. 9, no. 1, p. 12539, 2019.

[42] H.-Y. Wu, H.-C. Lin, Y.-H. Liu, K.-L. Chen, Y.-H. Wang, Y.-S. Sun, and J.-C. Hsu, "Highly sensitive, robust, and recyclable TiO_2/AgNP substrate for SERS detection," *Molecules*, vol. 27, no. 19, p. 6755, 2022.

[43] I. Sta, M. Jlassi, M. Hajji, M. F. Boujmil, R. Jerbi, and M. Kandyla, "Structural and optical properties of TiO_2 thin films prepared by spin coating," *Journal of Sol-Gel Science and Technology*, vol. 59, pp. 476–481, 2011.

[44] H. S. Ali, A. A. Al-Hassan, S. H. Al-Harthi, E. A. Al-Abbad, and A. Shaima, "Influence of thickness on the physical properties of nanostructured TiO_2 thin films," *Chalcogenide Letters*, vol. 17, no. 1, pp. 23–31, 2020.

[45] H. T. Nguyen, T. T. Le, V. T. Nguyen, T. T. Le, and N. T. Tran, "Annealing time effect on the structural, optical, and electrical properties of TiO_2 thin films prepared by spin coating," *Letters in Applied NanoBioScience,* vol. 134, p. 169, 2024.

[46] A. A. Hussein, A. S. Hassanien, and O. H. Abd-Elkader, "Effects of annealing temperature on structural, morphological, optical properties and photocatalytic activity of TiO_2 thin films," *Journal of Engineering and Applied Science*, vol. 11, pp. 4047–4053, 2016.

[47] Z. Wang, Y. Hu, Y. Zhang, L. Yang, Y. Gu, and S. Wang, "Effect of microstructure of TiO_2 thin films on optical band gap energy," *Chinese Physics Letters*, vol. 22, no. 7, pp. 1727–1729, 2005.

[48] Z. M. Rosli, and N. D. Johari, "Band gap energy and photo-catalytic efficiency of TiO_2 thin films deposited via dip and spin coating under visible light," *Journal of Power and Energy Engineering*, vol. 13, no. 12, pp. 1–13, 2025.

[49] M. H. Mithun, A. Sayed, and I. Rahaman, "The effect of band-gap on TiO_2 thin film considering various parameters," *Proceedings of Engineering and Technology Innovation*, vol. 19, pp. 45–52, 2021.

[50] Y. Li, Y. Wang, Y. Zhang, Y. Liu, and L. Zhang, "The charge transfer effect on SERS in a gold-decorated surface defect anatase nanosheet/methylene blue (MB) system," *Journal for new directions in chemistry*, vol. 45, no. 45, pp. 20952–20959, 2021.

[51] G. Singh, A. Kumar, R. Kumar, and P. Singh, "Deciphering the role of carbon quantum dots-metal heterojunction in SERS enhancement for methylene blue detection," *Journal of Applied Physics*, vol. 138, no. 20, p. 203103, 2025.

[52] Y. Zhang, Y. Liu, J. Li, and Z. Wang, "TiO_2 thickness-dependent charge transfer in an ordered Ag/TiO_2/Ni nanopillar arrays hybrid substrate," *Nanomaterials*, vol. 12, no. 10, p. 1688, 2022.

[53] S. Adesoye, and K. Dellinger, "ZnO and TiO_2 nanostructures for surface-enhanced Raman scattering-based bio-sensing: A review," *Sensing and Bio-Sensing Research*, vol. 37, p. 100499, 2022.

[54] S. Li, S. Yang, Y. Chen, L. Sun, H. Zhang, and H. Xu, "TiO_2 compact layer induced charge transfer enhancement in three-dimensional TiO_2-Ag SERS substrates," *Journal of Materials Chemistry C*, vol. 11, no. 14, pp. 4972–4981, 2023.

[55] X. Zhang, J. Li, Y. Liu, and H. Wang, "TiO_2 nanofoam-nano-tube array for surface-enhanced Raman spectroscopy," *ACS Applied Nano Materials*, vol. 1, no. 11, pp. 6115–6122, 2018.

[56] E. C. Le Ru, and P. G. Etchegoin, *Principles of Surface-Enhanced Raman Spectroscopy and Related Plasmonic Effects*. Amsterdam, The Netherlands: Elsevier, p.185, 2009.

[57] S. Schlücker, "Surface-enhanced raman spectroscopy: concepts and chemical applications," *Angewandte Chemie International Edition*vol. 53, no. 19, pp. 4756–4795, 2014.

[58] J. Langer, D. J. de Aberasturi, J. Aizpurua, R. A. Alvarez-Puebla, J. J. Baumberg, S. I. Bozhevolnyi, and L. M. Liz-Marzan, "Present and future of surface-enhanced Raman scattering," *ACS Nano*, vol. 14, no. 1, pp. 28–117, 2020.

[59] B. Santara, P. K. Giri, K. Imakita, and M. Fujii, "Evidence for Ti interstitial induced extended visible absorption and near infrared photoluminescence from undoped TiO_2 nanoribbons: An *in situ* photoluminescence study," *Journal of Physical Chemistry C*, vol. 117, no. 23, pp. 23402−23411, 2013.

[60] D. K. Pallotti, L. Passoni, P. Maddalena, F. Di Fonzo, and S. Lettieri, "Photoluminescence mechanisms in anatase and rutile TiO_2," *Journal of Physical Chemistry C*, vol. 121, no. 15, pp. 9011–9021, 2017.